ENERGY TRANSFER IN EUROPIUM DOPED POTASSIUM CHLORIDE

By

LARRY DEAN MERKLE II

Bachelor of Science

Oklahoma State University

Stillwater, Oklahoma

1974

Submitted to the Faculty of the Graduate College
of the Oklahoma State University
in partial fulfillment of the requirements
for the Degree of
MASTER OF SCIENCE
May, 1976

ENERGY TRANSFER IN EUROPIUM DOPED

POTASSIUM CHLORIDE

Thesis Approved:

Richard C. Powell
Thesis Adviser

Joel J. Martin

W. A. Sibley

A. N. Duncan
Dean of Graduate College

ACKNOWLEDGEMENTS

I wish to express my appreciation to my thesis adviser, Dr. R. C. Powell, for his patient guidance and encouragement throughout this study. Thanks are also due the members of my committee, Dr. W. A. Sibley and Dr. J. J. Martin, for their help and advice, and particularly for Dr. Martin's considerable aid in elucidating for me some of the mysteries of europium aggregation in these crystals.

TABLE OF CONTENTS

LIST OF TABLES

LIST OF FIGURES

CHAPTER I

INTRODUCTION

Time Resolved Spectroscopy in Energy Transfer Studies

The development of time resolved spectroscopy has provided a very simple and direct tool for the study of energy transfer in solids. Using a laser pulse of very short duration as an excitation source, the variation with time of the resulting sample fluorescence may be observed. Indeed, if a boxcar integrator with proper gating is employed, a particular time after the laser pulse may be chosen for scrutiny. This time resolution capability affords the investigator an opportunity to observe the time-evolution of the entire fluorescence spectrum.

The value of this technique in energy transfer studies lies in its relation to the rate of transfer and the dependence upon time of the number of excited atoms or ions involved in the transfer. From the time-evolution of the fluorescence spectrum this dependence upon time is readily accessible by observation of linewidths and relative intensities of fluorescence lines emanating from the types of ions involved in the transfer. Not only may the general form of this time dependence indicate the type of transfer mechanism present, but the quantitative analysis of the results indicates the strength of the interaction. Time resolved spectroscopy thus gives an easier and more sensitive way of characterizing energy transfer than the usual investigations of the concentration

and temperature dependences of the transfer rate.

Europium Doped Potassium Chloride

Potassium chloride doped with divalent europium was chosen for this study to complement other work being done on this material in the Oklahoma State University Department of Physics. Primary interest in the material is investigation of its feasibility as a window for carbon dioxide lasers, involving optical absorption and mechanical strengths measurements. Its possible applicability as a laser window owes in part to its lack of absorption at the wavelength of the carbon dioxide laser. The divalent europium does absorb strongly in the 2000Å to 4500Å region however, and it was in this region that this study was made.

The electronic transition which gives rise to this absorption is $4f^7$ to $4f^6 5d$, which has been observed by Reisfeld and Glasner[1] as producing two broad absorption bands separated by about 11,000 cm^{-1}. This two-band absorption has also been observed for Eu^{2+} in other host crystals, the splitting generally being attributed to the crystal field splitting of the free ion 5d orbital into e_g and t_{2g} crystal field orbitals, while the breadth and low temperature structure of each band is attributed to the spin-orbit splitting of the $4f^6$ configuration[2], or to the Coulomb interaction between the 5d and the $4f^6$ electrons[3]. However, Kisliuk, Tippins, Moore, and Pollack[4] have indicated that the spin-orbit, the crystal field, and the 5d-$4f^6$ Coulomb interaction terms must all be considered, none being small enough to neglect. A similar conclusion is reached by Weakliem[5], who notes that while the splitting of the 5d level by the cubic crystal field considered by him is quite large the crystal field should have little effect on the $4f^6$ core, which is thus split

primarily by the other interactions.

Divalent impurities such as europium must be associated with a charge compensator when in a host whose cations are monovalent as in KCl. In a chemically pure crystal this charge compensator is usually a cation vacancy, as no other compensators are available. Fong[6,7] has done considerable work on the relative probabilities of various locations of the vacancy with respect to the divalent cation in an alkali-halide host. This work, largely concerned with samarium but also dealing with divalent rare earths generally, shows that the nearest-neighbor cation sites are the most probable sites for the vacancy but that it may also reside somewhat farther from the impurity ion with small but non-negligible probability at room temperature. The proximity of such a vacancy to a divalent europium ion in KCl lowers the symmetry of the site, which would otherwise be cubic.

The fluorescence spectra of Eu^{2+} in many crystals consist of a sharp line with an associated low-energy side band[2]. This sharp line, seen at approximately 4105Å for KCl:Eu^{2+} by Tamura and co-workers[8], has been identified as the transition from the lowest lying level of the $4f^6 5d$ configuration to the $^8S_{7/2}(4f^7)$ ground state[2]. The side band, attributed to vibronic interactions, has been studied for KCl and other alkali-halide hosts by Tamura[8]. However, vibronic considerations will be of little concern in this work.

Summary of Thesis

In this study time resolved spectroscopy is used to investigate and characterize energy transfer among divalent europium ions in crystalline potassium chloride. Data include room temperature absorption and

low temperature excitation spectra, as well as room temperature and low temperature spectra of the broad fluorescence band characteristic of this material. Other data presented are low temperature spectra and lifetimes of the observed zero phonon fluorescence lines in two samples, one annealed and quenched and the other untreated. From these data the lines are identified as arising from europium ions in different crystal field sites. A model is proposed to explain the observed time dependence of the relative intensities of two of the zero phonon lines at two temperatures. The model, which assumes resonant energy transfer among europium ions, is shown to fit the data qualitatively and to be more reasonable than other possible models. From the quantitative fit of the data the energy transfer rate is found and shown to give reasonable agreement with the theoretically predicted rate for electric dipole-dipole resonant transfer.

CHAPTER II

THEORETICAL BACKGROUND

In the study of energy transfer in solids one kind of atom or ion is excited and this excitation energy is passed to another kind of ion from which the energy is emitted. The kind which is originally excited is called the sensitizer and the kind which emits the energy after transfer is referred to as the activator.

Several mechanisms may cause energy transfer between ions. One of the more important is resonant transfer by electric or magnetic multipole interaction. This work is primarily concerned with the electric dipole-dipole interaction.

Electric Dipole-dipole Transfer Rate

The rate of electric dipole-dipole transfer of excitation energy may be derived from the "golden rule" of time dependent perturbation theory, using a multipole expansion of the electrostatic interaction to find the needed Hamiltonian. Following the development of Dexter[9], the transfer may be expressed as a transition from state ψ_i, consisting of the excited sensitizer ψ_s' and the activator ground state ψ_a, to state ψ_f, comprising the sensitizer ground state ψ_s and the excited activator state ψ_a'. From the "golden rule" the transfer rate is thus given by

$$\omega_{sa} = \frac{2\pi}{\hbar} \rho_E \left| \int \psi_i^* \, H' \psi_f \right|^2, \tag{1}$$

where ρ_E is the final density of states and H' is the interaction Hamil-

tonian.

The energies of the initial and final states are not sharp, due to lattice vibrations. Thus, the density of states and the wave functions may be considered to be functions of a continuously variable energy. Defining $p'_s(w'_s)$ and $p_a(w_a)$ as the functions giving the probabilities of the sensitizer having initial energy w'_s and the activator having initial energy w_a respectively, the normalization of the initial state energies and wave functions is given by

$$\int |\psi'_s(w'_s)|^2 d\tau = \int |\psi_a(w_a)|^2 d\tau = 1 \tag{2}$$

and

$$\int_o^\infty p'_s(w'_s) dw'_s = \int_o^\infty p_a(w_a) dw_a = 1 \tag{3}$$

The sensitizer and activator energies of the final state are in the ranges w_s to $w_s + \Delta w$ and w'_a to $w'_a + \Delta w$, so that the final state wave functions are normalized

$$\frac{1}{\Delta w} \int_w^{w + \Delta w} dw_s \int |\psi_s(w_s)|^2 d\tau = 1 \tag{4}$$

and

$$\frac{1}{\Delta w} \int_w^{w + \Delta w} dw'_a \int |\psi'_a(w'_a)|^2 d\tau = 1 \tag{5}$$

The density of states ρ_E may be absorbed by the energy distribution functions p'_s and p_a if a Dirac delta is included for energy conservation. Further, the $1/\Delta w$ terms may be absorbed into the square of the matrix element, $|\langle H' \rangle|^2$, making it a unitless quantity. If the transfer probability is now summed over all possible initial and final states, the degeneracies of the initial sensitizer and activator states must be accounted for through division by g'_s and g_a, since only one of the degenerate states is actually occupied. The total probability now becomes

$$\omega_{sa} = \frac{2\pi}{\hbar} \sum_I \sum_F \frac{1}{g'_s g_a} \int dw'_a \int dw_s \int dw_a p_a(w_a) \int dw'_s p'_s(w'_s) \left| \langle H'(w'_s, w_a; w_s, w'_a) \rangle \right|^2$$

$$\delta(w'_s + w_a - w_s - w'_a). \tag{6}$$

Using the Dirac delta to integrate over w_s and defining $E = w'_a - w_a = w'_s - w_s$,

$$\omega_{sa} = \frac{2\pi}{\hbar} \sum_I \sum_F \frac{1}{g'_s g_a} \int dE \int dw_a p_a(w_a) \int dw'_s p'_s(w'_s) \left| \langle H'(w'_s, w_a; w'_s - E, w_a + E) \rangle \right|^2. \tag{7}$$

The interaction Hamiltonian desired for this study is the dipole part of the energy H of a charge distribution $\rho(\vec{r})$ due to an external dipole potential field $\phi(\vec{r})$:

$$H = \int \rho(\vec{r}) \, \phi(\vec{r}) \, d\tau. \tag{8}$$

If the activator has N electrons and M - N protons then

$$\rho(\vec{r}) = \sum_{i=1}^{N} (-e)\delta(\vec{r} - \vec{r}_{ai}) + \sum_{i=N+1}^{M} e\delta(\vec{r} - \vec{r}_{ai}) = \sum_{i=1}^{M} q_i \delta(\vec{r} - \vec{r}_{ai}). \tag{9}$$

The potential field may be expanded about the center of mass of the activator, $\vec{R}$, to give

$$\phi(\vec{r}_{ai}) = \phi(\vec{R}) + \vec{r}_{ai} \cdot \nabla\phi(\vec{R}) + \ldots$$

$$= \phi(\vec{R}) - \vec{r}_{ai} \cdot \vec{E}(\vec{R}) + \ldots \tag{10}$$

For the interaction Hamiltonian only the dipole term is desired, so that

$$H' = \sum_{i=1}^{M} (-q_i)\vec{r}_{ai} \cdot \vec{E}(\vec{R}), \tag{11}$$

or writing the net dipole moment of the activator as $\vec{p}_a = e\vec{r}_a = \sum_i q_i \vec{r}_{ai}$,

$$H' = -e\vec{r}_a \cdot \vec{E}(\vec{R}). \tag{12}$$

For electric dipole-dipole interaction only the dipole term of the external field is regarded as important. Therefore

$$\vec{E}(\vec{R}) = \frac{3\hat{R}(\vec{p}_s \cdot \hat{R}) - \vec{p}_s}{\kappa R^3} \tag{13}$$

where κ is the relative permeability and the sensitizer dipole moment definition is analogous to that of the activator dipole moment. Therefore, the dipole-dipole interaction Hamiltonian is

$$H' = \frac{e^2}{\kappa R^3}\{\vec{r}_a \cdot \vec{r}_s - 3(\vec{r}_a \cdot \hat{R})(\vec{r}_s \cdot \hat{R})\}, \tag{14}$$

so that

$$\omega_{sa} = \frac{2\pi e^4}{\hbar \kappa^2 R^6} \sum_I \sum_F \frac{1}{g_s' g_a} \int dE \int dw_a p_a(w_a) \int dw_s' p_s'(w_s')$$

$$\left|\langle\vec{r}_s\rangle \cdot \langle\vec{r}_a\rangle - 3(\langle\vec{r}_s\rangle \cdot \hat{R})(\langle\vec{r}_a\rangle \cdot \hat{R})\right|^2. \tag{15}$$

An average over all orientations of $\langle\vec{r}_s\rangle$ and $\langle\vec{r}_a\rangle$ is now taken, using the definitions: θ is the angle between $\langle\vec{r}_a\rangle$ and $\vec{R}$, θ' is the angle between $\langle\vec{r}_s\rangle$ and $\vec{R}$, and ϕ is the asimuthal angle of $\langle\vec{r}_s\rangle$ relative to that of $\langle\vec{r}_a\rangle$. Thus,

$$\langle\vec{r}_s\rangle \cdot \langle\vec{r}_a\rangle - 3(\langle\vec{r}_s\rangle \cdot \hat{R})(\langle\vec{r}_a\rangle \cdot \hat{R}) = |\langle\vec{r}_s\rangle||\langle\vec{r}_a\rangle|\{\cos\theta\cos\theta' +$$

$$\sin\theta\sin\theta'\cos\phi - 3\cos\theta\cos\theta'\} = |\langle\vec{r}_s\rangle||\langle\vec{r}_a\rangle|\phi. \tag{16}$$

Therefore

$$\omega_{sa} = \frac{2\pi e^4}{\hbar \kappa^2 R^6} \sum_I \sum_F \frac{1}{g_s' g_a} \int dE \int dw_a p_a(w_a) \int dw_s' p_s'(w_s') |\langle\vec{r}_a\rangle|^2 |\langle\vec{r}_s\rangle|^2 \langle|\phi|^2\rangle_{ave} \tag{17}$$

where the average of $|\phi|^2$ over all θ, θ', and ϕ is

$$\langle|\phi|^2\rangle_{ave} = \langle|\sin\theta\sin\theta'\cos\phi - 2\cos\theta\cos\theta'|^2\rangle_{ave} = 2/3 \tag{18}$$

It should be noted that the units of $\langle\vec{r}\rangle^2$ are length squared per unit energy. Denoting the specific energy states involved in $\langle\vec{r}_a\rangle$ by rewrit-

ing it $\langle \vec{r}_a(w_a, w_a + E) \rangle$ and similarly writing $\langle \vec{r}_s \rangle$ as $\langle \vec{r}_s(w_s', w_s' - E) \rangle$, the transition probability per unit time for dipole-dipole transfer is

$$\omega_{sa} = \frac{4\pi e^4}{3\hbar\kappa^2 R^6} \sum_{i,f} \frac{1}{g_s' g_a} \int dE \left\{ \int dw_s' p_s'(w_s') \left| \langle \vec{r}_s(w_s', w_s' - E) \rangle \right|^2 \right\}$$

$$\left\{ \int dw_a p_a(w_a) \left| \langle \vec{r}_a(w_a, w_a + E) \rangle \right|^2 \right\}. \tag{19}$$

The Einstein A(E) coefficient, the emission probability distribution over energy E, is

$$A(E) = \frac{4e^2 E^3}{3\hbar^4 c^3} \left| \langle \psi_f | \vec{r} | \psi_i \rangle \right|^2 \tag{20}$$

for an isolated atom with only the electric dipole Hamiltonian considered. In a crystal this quantity is modified by inclusion of a probability function for the broadened energy levels and by the ratio $(\varepsilon_c/\varepsilon)^2$ which expresses the modification of the electric field by the crystal, coming in squared due to the squaring of the matrix element. Also, since the probability includes $k^2 dk$ and k is multiplied by the index of refraction n in a crystal, a factor of n^3 enters. Summing over all possible transitions resulting in energy change E and dividing out the degeneracy as before, the result is

$$A(E) = \sum_i \sum_f \frac{4e^2 E^3}{3\hbar^4 c^3 g'} \left(\frac{\varepsilon_c}{\varepsilon}\right)^2 n^3 \int \left| \langle r_{if}(w', w' - E) \rangle \right|^2 p'(w') dw'. \tag{21}$$

Similarly the Einstein B coefficient, the probability distribution for absorption, is

$$B(E) = \sum_i \sum_f \frac{2\pi e^2}{3\hbar^2 g} \left(\frac{\varepsilon_c}{\varepsilon}\right)^2 \int \left| \langle r_{if}(w, w + E) \rangle \right|^2 p(w) dw. \tag{22}$$

Since A is the probability distribution for decay, its integral over E equals $1/\tau$, where τ is the radiative lifetime of the excited atom. Thus, a normalized function f(E) may be defined, having the emission

lineshape and such that its integral over E is unity. Then

$$\sum_i \sum_f \int |\langle r_{if}(w', w' - E)\rangle|^2 p'(w')dw' = \frac{3\hbar^4 c^3 g'}{4n^3 e^2 E^3} \left(\frac{\varepsilon}{\varepsilon_c}\right)^2 \frac{f(E)}{\tau}. \tag{23}$$

Noting that the photon velocity in a crystal is c/n, the absorption cross section of an impurity is

$$\sigma(E) = \frac{2\pi\hbar E}{c/n} B(E) \tag{24}$$

If this cross section is integrated over E to give Q and a normalized function of the same shape, F(E), is introduced, the result is

$$\sum_i \sum_f \int |\langle r_{if}(w, w + E)\rangle|^2 p(w)dw = \frac{3\hbar cg}{4\pi^2 e^2 hE} \left(\frac{\varepsilon}{\varepsilon_c}\right)^2 QF(E). \tag{25}$$

With these substitutions for the sensitizer emission and the activator absorption, the rate of dipole-dipole transfer is

$$\omega_{sa} = \frac{3c^4\hbar^4 Q_a}{4\pi\kappa^2 n^4 R^6 \tau_s} \left(\frac{\varepsilon}{\varepsilon_c}\right)^4 \int \frac{f_s(E)F_a(E)}{E^4} dE. \tag{26}$$

Grouping factors together to the customary form gives the result

$$\omega_{sa} = \frac{1}{\tau_s} (R_o/R)^6. \tag{27}$$

Time Dependence of Transfer to Random Sites

If a crystal has random distributions of both sensitizer and activator sites the rate of decay of an excited sensitizer is its radiative decay rate, τ, plus an energy transfer rate characteristic of its activator environment. That is, all sensitizers with the same distribution of unexcited activators around them decay at the same rate. Define class c as the class of sensitizers with the same environment of activators,

N_s as the number of sensitizers, N_c as the number of sensitizers in class c, n_c^* as the number in class c which are excited, and N_a as the number of activators. Further, let ω_c be the energy transfer rate to activators from a class c sensitizer, and let R_i equal the distance of a sensitizer from activator i. Then for electric dipole-dipole interaction

$$\omega_c = \frac{1}{\tau} \sum_{i=1}^{N_a} \left(\frac{R_o}{R_i}\right)^6 \tag{28}$$

If initial excitation is accomplished by a very short pulse at $t = 0$, then for later times

$$\frac{dn_c^*}{dt} = -\frac{1}{\tau} n_c^* - \omega_c n_c^*. \tag{29}$$

Therefore,

$$n_c^*(t) = n_c^*(0) e^{-(1/\tau + \omega_c)t}. \tag{30}$$

Defining $P_c(dc)$ as the probability of a sensitizer having environment c,

$$N_c = N_s P_c(dc). \tag{31}$$

Since the orientations of sensitizer and activator dipoles have already been averaged into ω_{sa} and so into R_o, the probability of a sensitizer seeing environment c is just the product of probabilities of an activator being a distance R_i from the sensitizer, the product being over all N_a activators. The probability of an activator being a distance R_i away is, in turn, just the fraction of the total volume V of the crystal within a thin spherical shell of radius R_i: $4\pi R_i^2 dR_i/V$. Therefore,

$$P_c(dc) = \prod_{i=1}^{N_a} \frac{4\pi R_i^2 dR_i}{V} \tag{32}$$

which with Equations (30) and (31) gives

$$n_c^*(t) = kN_s e^{-(1/\tau + \omega_c)t} \prod_{i=1}^{N_a} \frac{4\pi R_i^2 dR_i}{V} \tag{33}$$

where k is the fraction of sensitizers originally excited. The total number of excited sensitizers, $n^*(t)$, is thus

$$n^*(t) = kN_s \int_{N_a} \cdots \int e^{-(1/\tau + \omega_c)t} \prod_{i=1}^{N_a} \frac{4\pi R_i^2 dR_i}{V}$$

$$= kN_s e^{-t/\tau} \int \cdots \int \prod_i e^{-t/\tau (R_o/R_i)^6} \frac{4\pi R_i^2 dR_i}{V}$$

$$= kN_s e^{-t/\tau} (I)^{N_a}, \tag{34}$$

where

$$I = \int_o^{R_v} e^{-t/\tau (R_o/R)^6} \frac{4\pi R^2 dR}{V} \tag{35}$$

and $4\pi R_v^3/3 = V$.

To evaluate I let $x = (R_o/R)^6 t/\tau$ and note that for times of interest t is no larger than a few τ. Thus

$$R^2 dR = -\frac{R_o^3 t^{1/2}}{6\tau^{1/2} x^{3/2}} dx \tag{36}$$

and

$$I = \int_{x=\infty}^{x_v} e^{-x} \cdot \frac{-4\pi R_o^3 t^{1/2}}{6\tau^{1/2}} \left(\frac{3}{4\pi R_v^3}\right) x^{-3/2} dx = \tfrac{1}{2} x_v^{1/2} \int_{x_v}^{\infty} e^{-x} x^{-3/2} dx, \tag{37}$$

where $x_v = (R_o/R_v)^6 t/\tau$. Integrating by parts,

$$I = \tfrac{1}{2} x_v^{1/2} [2e^{-x_v} x_v^{-1/2} - 2\int_{x_v}^{\infty} e^{-x} x^{-1/2} dx] = e^{-x_v} - x_v^{1/2} [\int_o^{\infty} e^{-x} x^{-1/2} dx - \int_o^{x_v} e^{-x} x^{-1/2} dx] \tag{38}$$

For almost any crystalline sample $R_v \gg R_o$, so that for any time of

interest $x_v << 1$. Therefore,

$$I = 1 - x_v + \ldots - (\pi x_v)^{\frac{1}{2}} + x_v^{\frac{1}{2}} \int_o^{x_v} (x^{-\frac{1}{2}} - x^{\frac{1}{2}} + \ldots) dx$$

$$\doteq 1 - x_v - (\pi x_v)^{\frac{1}{2}} + 2x_v$$

$$= 1 - (\pi x_v)^{\frac{1}{2}} + \text{higher order terms.} \tag{39}$$

Thus

$$I \doteq 1 - \frac{4\pi^{3/2} t^{\frac{1}{2}}}{3V\tau^{\frac{1}{2}}} R_o^3. \tag{40}$$

Since $x_v << 1$,

$$(I)^{N_a} \doteq (1 - \frac{4\pi^{3/2} R_o^3}{3V} \cdot \frac{t^{\frac{1}{2}}}{\tau^{\frac{1}{2}}})^{N_a}$$

$$\doteq \exp(-N_a 4\pi^{3/2} R_o^3 t^{\frac{1}{2}} / 3V\tau^{\frac{1}{2}}) \tag{41}$$

so that

$$n^*(t) = kN_s \exp(-t/\tau - N_a 4\pi^{3/2} R_o^3 t^{\frac{1}{2}} / 3V\tau^{\frac{1}{2}}). \tag{42}$$

The total rate of transfer from the sensitizer population, defined as $\omega_r(t)$ in the expression

$$n^*(t) = kN_s e^{-(t/\tau + \omega_r t)}, \tag{43}$$

is therefore

$$\omega_r = \omega_r(t) = 4\pi^{3/2} R_o^3 Ca / 3(\tau t)^{\frac{1}{2}}, \tag{44}$$

where $C_a = N_a/V$ is the activator concentration.

Diffusion Transfer Rate

If there are far more sensitizers than activators in a cyrstal, the proximity of many unexcited sensitizers to an excited sensitizer may make it probable that excitation energy migrate for many steps among

sensitizers before reaching an activator. If the activator is modeled as a perfectly absorbing trap the migration of quanta of excitation energy, or excitons, may be described by a random walk model or by a diffusion equation. In the limit of many steps in the random walk the two descriptions give consistent results [10].

The equation describing the rate of change of the exciton population in the diffusion formulation is

$$\frac{\partial N(r,t)}{\partial t} = W(t) - BN(r,t) + D\,\nabla^2 N(r,t) \tag{45}$$

where $N(r,t)$ is the exciton concentration, B is the sensitizer decay rate, D is the diffusion coefficient, and $W(t)$ is the rate of excitation of sensitizers. A convenient initial condition is $N(r,0) = 0$, and if the simple case of one single trap of radius R located at the origin is considered, an appropriate boundary condition is $N(R,t) = 0$. With the substitution

$$N(r,t) = \frac{u(r,t)}{r}\, e^{-Bt}, \quad r>R \tag{46}$$

the rate equation becomes

$$\frac{\partial u(r,t)}{\partial t} = W(t) r e^{Bt} + D\,\frac{\partial^2 u}{\partial r^2}. \tag{47}$$

If $W(t) = N_o \delta(t)$, the Laplace transform of the rate equation is

$$s\tilde{u}(r,s) - u(t=0) = rN_o + D\frac{\partial^2 \tilde{u}}{\partial r^2}. \tag{48}$$

Upon application of the boundary conditions and requirement that the solution stay finite,

$$\tilde{u}(s) = \frac{-N_o R}{s}\, e^{-(r-R)s^{1/2}/D^{1/2}} + \frac{N_o r}{s} \tag{49}$$

so that

$$N(r,t) = N_o\left[1 - \frac{R}{r}\,\mathrm{erfc}\,\left(\frac{r-R}{2D^{1/2}t^{1/2}}\right)\right]e^{-Bt} \tag{50}$$

The flux of excitons crossing the spherical surface of a single trap is

$$F_1(t) = 4\pi R^2 D \frac{\partial N}{\partial r}\Big|_{r=R}$$

$$= 4\pi R^2 D\left[\frac{1}{R} + \frac{1}{(\pi Dt)^{\frac{1}{2}}}\right] N_o e^{-Bt}. \tag{51}$$

For N_t non-interacting traps,

$$F_N(t) = 4\pi D N_o N_t e^{-Bt}\left[R + \frac{R^2}{(\pi Dt)^{\frac{1}{2}}}\right]. \tag{52}$$

Far from any traps the exciton concentration would be simply $N_o e^{-Bt}$, so the flux is simply this concentration times the rate, k(t), of transfer into traps. Thus

$$k(t) = 4\pi D N_t R\left(1 + \frac{R}{(\pi Dt)^{\frac{1}{2}}}\right), \tag{53}$$

and since the time dependent term usually becomes small very quickly, the rate for times of interest is

$$k = 4\pi D N_t R. \tag{54}$$

Thus, the diffusion transfer rate is constant for most times of interest.

CHAPTER III

EXPERIMENTAL BACKGROUND

Crystal Growth

The europium doped potassium chloride crystals used in this study were grown in the Oklahoma State University crystal growth facility, in part by the author. Small quantities of europium trichloride were first mixed with reagent grade KCl. The mixture was purified in a Bridgman-Stockbarger furnace by a reactive atmosphere processing technique. In this technique argon is bubbled through carbon tetrachloride and passed over an open-topped crucible containing the salts throughout the melting and slow cooling of the Bridgman crystal growth process. The slow refreezing of the melt effectively zone-refines the KCl, and the reactive atmosphere aids in removal of OH^- and O_2^-, which tend to be the most serious contaminants of these crystals if not processed in this way. The final OH^- concentration is on the order of 0.1 ppm atomic, and although the O_2^- concentration has not been precisely measured it is also believed to be quite low, as evidenced by very low absorption of 10.6 μm light[11].

The purified material was then used as starting material for growth of single crystals by the Kyropoulos-Czochralski method. After thorough evacuation of the growth furnace by diffusion pump the salts were melted in an argon atmosphere of about 100 torr to suppress evaporation. Seeds

were either previously grown KCl:Eu^{2+} or pure KCl, positioned such that growth was along a <100> direction. The crystals were pulled from the melt over a period of several hours. After growth the temperature of the furnace was programmed down to room temperature overnight, thus accomplishing some degree of annealing.

The resulting single crystals exhibit optical absorption and fluorescence characteristic of Eu^{2+}, the reduction from the trivalent state resulting from the high temperatures of the purification and growth processes. The europium solubility in KCl proved to be rather low, with the result that europium concentrations in the crystals seldom exceeded 500 ppm atomic as measured by optical absorption at room temperature.

Sample Properties

As discussed previously, a divalent cation in an alkali-halide lattice must be charge compensated by a negative impurity or an alkali vacancy. In the KCl:Eu^{2+} samples grown at this university, the impurity anion concentration is sufficiently low that the K^+ vacancy should be the predominant charge compensator[11]. Electron spin resonance data indicate that one site symmetry for the Eu^{2+}, that corresponding to the nearest neighbor vacancy position, is the predominant site symmetry[12]. The data do not exclude the possibility that very small numbers of ions may be at sites of other symmetries.

It is known that the vacancies in such vacancy compensated alkali-halide crystals are quite free to move at or above room temperature, by changing places with a neighboring cation[7]. Since this position exchange may involve a divalent impurity cation the mobility of the vacancies affords a certain degree of mobility to the impurities as well. This

effect is evidenced by the slow clustering, due to the net attractive electric interaction between divalent cation-vacancy pairs, of the impurities and their charge compensating vacancies into dimers, trimers, or larger clusters[13]. Such clustering has been observed, for example, by Sundberg, Lauer, and Fong in NaCl:Sm^{2+} [14]. Mechanical strengths data indicate that such clustering also takes place in KCl:Eu^{2+} [11]. Concentration dependence of flow stress data is characteristic of isolated europium-vacancy pairs for samples recently quenched from high temperatures, about 600°C, to room temperature. However, data taken on samples left at room temperature for some time indicate a behavior progressively more consistent with the formation of clusters of the cation-vacancy pairs. This change occurs over a period of a few weeks. Room temperature absorption spectra are not changed by the annealing and quenching process. This may be expected, however, since the energy level perturbation caused by differing site symmetries or by proximity of another europium ion is expected to be small, owing to the shielding of the 4f level by the 5s and 5p electrons.

The samples used in this study were cleaved from a boule of KCl:Eu^{2+} with a europium concentration of about 275 ppm atomic as measured by comparison of room temperature absorption with a previously prepared calibration curve. All time dependent data were taken on a sample which was quenched from 600°C to room temperature,then kept at 77 K overnight to retard reappearance of clusters before the taking of data the following day. Fluorescence spectra were also taken for a sample from the same boule which had been at room temperature for several months. Comparison of samples thought to be in the clustered state with those in a relatively cluster free condition could thus be made.

Apparatus

Absorption spectra were taken on a Cary 14 spectrometer, using both the visible and ultraviolet light sources. All absorption data were taken at room temperature.

Excitation spectra were made using as a source a 150 W xenon lamp, model X150 from PEK, Inc. The light was focused onto the entrance slit of a Spex model 1670 minimate monochromator, with slit width typically 1.25 mm to 2.50 mm. A short focal length lens focused the monochromator output onto the sample. The apparatus for detection of the fluorescence was positioned at right angles to the path of exciting light and included a PAR model 125 mechanical light chopper operating at 2000 Hz and a lens system to focus the signal onto the entrance slit of a Spex one meter Czerny-Turner spectrometer. This spectrometer, model 1704, has 4Å per mm dispersion and ultimate resolution better than 0.1Å, and was used with slit widths of about 0.25 mm for excitation spectra. An RCA C31034 phototube cooled by a Products for Research thermoelectrically refrigerated chamber, model TE-104, was mounted at the exit slit of the spectrometer as a detector.

For fluorescence spectra and lifetime measurements an AVCO Everett model C400 pulsed nitrogen laser was the excitation source. The output of this laser is an ultraviolet line of wavelength 3371Å and half width less than 4Å, with effective pulsewidth of 5 nanoseconds. The pulse rate is continuously variable from 1 Hz to 100 Hz, and was used near 10 Hz throughout this study. The laser output was focused onto the sample, the fluorescence of which was focused onto the Spex one meter spectrometer entrance slit. The spectrometer slit widths were 10 microns when used with the laser.

For all low temperature measurements the sample to be studied was mounted on the cold finger of an Air Products and Chemicals model CS-202 Displex Cryogenic Refrigerator, a closed cycle helium refrigerator. Thermal contact between the sample and the cold finger was aided by application of a small amount of Air Products Cry-con conducting grease, carefully positioned behind the mounting clips holding the sample to avoid excitation of the grease by the excitation source and any resulting fluorescence. This cryogenic system typically attains a low temperature of about 13 K, as measured by a chromel vs. gold-0.07 at. percent iron thermocouple.

The output of the phototube was processed by a Princeton Applied Research Corp. model 162 Boxcar Averager with two model 164 gated integrator modules. The signal was fed into the one megohm input of the boxcar in parallel with a variable resistor. Reduction of the value of this resistance shortens the response time of the system, but also lowers the signal received by the boxcar. Consequently it was adjusted to insure that the system response time did not distort the time dependence of the fluorescence, but without unnecessary signal reduction. The integrator system, when triggered by the pulsed laser or the chopper, samples the phototube signal during a narrow aperture which may be fixed at any time after the triggering pulse or may be scanned across a wide time range. The signal which passes the aperture is applied to an integrator of variable time constant so that the output is the average of a number of pulses of the input signal, thus improving the signal to noise ratio. The width of the aperture may be varied from 5 ns to 0.5 ms, whereas the position of the aperture may be varied independently for the two channels from about 5 ns to 50 ms after the triggering pulse.

The minimum possible delay time is limited by the aperture width selected. In the scanning mode the range of scan may be chosen from 100 ns to 50 ms, with the time required for one scan variable from 0.01 sec to 10^5 sec.

Two applications of the various modes of operation of the boxcar averager are of importance in this work. For measurement of lifetimes the spectrometer was set on the desired fluorescence wavelength and the boxcar aperture was scanned with a typical range setting of 5 μs or 10 μs. For the recording of spectra the aperture was fixed at a specific time after pulse while the spectrometer was scanned over the desired range of wavelengths. In this way spectra, plotted on a Heath strip chart recorder, were observable as a function of time after laser pulse.

The apparatus for time resolved spectroscopy, including laser, cryostat, spectrometer, photomultiplier tube, boxcar averager, and recorder, is shown in Figure 1.

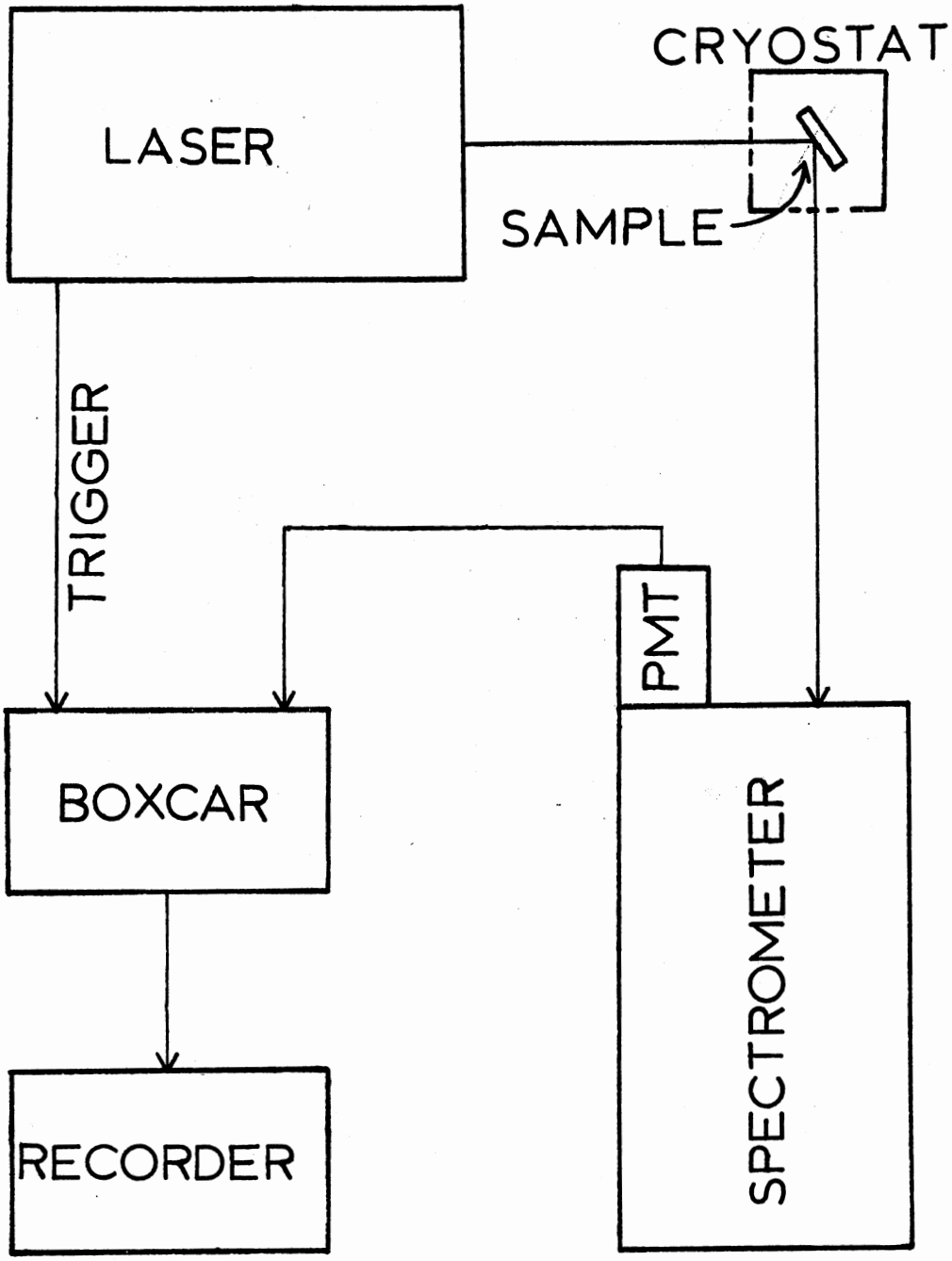

Figure 1. TRS Apparatus

CHAPTER IV

EXPERIMENTAL RESULTS

Spectra and Lifetimes

The room temperature absorption spectrum of a 0.67 mm thick sample of KCl:Eu^{2+} is shown in Figure 2. The spectrum exhibits two strong absorption bands, one with peak at about 2400Å showing no structure and the other with peak at 3300Å and a distinct shoulder at about 3650Å. The optical density at the peak of the lower energy band is 0.466, corresponding to a europium concentration of 275 ppm atomic, or approximately 4.40×10^{18} cm^{-3}, by comparison with a calibration curve.

The excitation spectrum at T = 13 K with fluorescence monitored at 4350Å is shown in Figure 3. The spectrum has peaks at 4000Å, 3800Å, 3540Å, and 3370Å, and a small shoulder at about 3200Å. Scattered light began reaching the phototube at 4300Å, implying a resolution of about 50Å.

The fluorescence of KCl:Eu^{2+} for excitation at 3371Å exhibits a broad band which peaks near 4200Å at room temperature and also at 15 K. Figure 4 shows no structure for the room temperature fluorescence band, whereas the fluorescence at 15 K for a sample quenched from 600°C on the previous day exhibits large peaks at 4108Å, 4142Å, and 4173Å and smaller peaks at 4116Å, 4125Å, 4128Å, 4132Å, and 4150Å. Less well resolved structure is seen at about 4190Å, 4203Å, and 4238Å. The intensity, narrow linewidth and position of the 4108Å line suggest it as

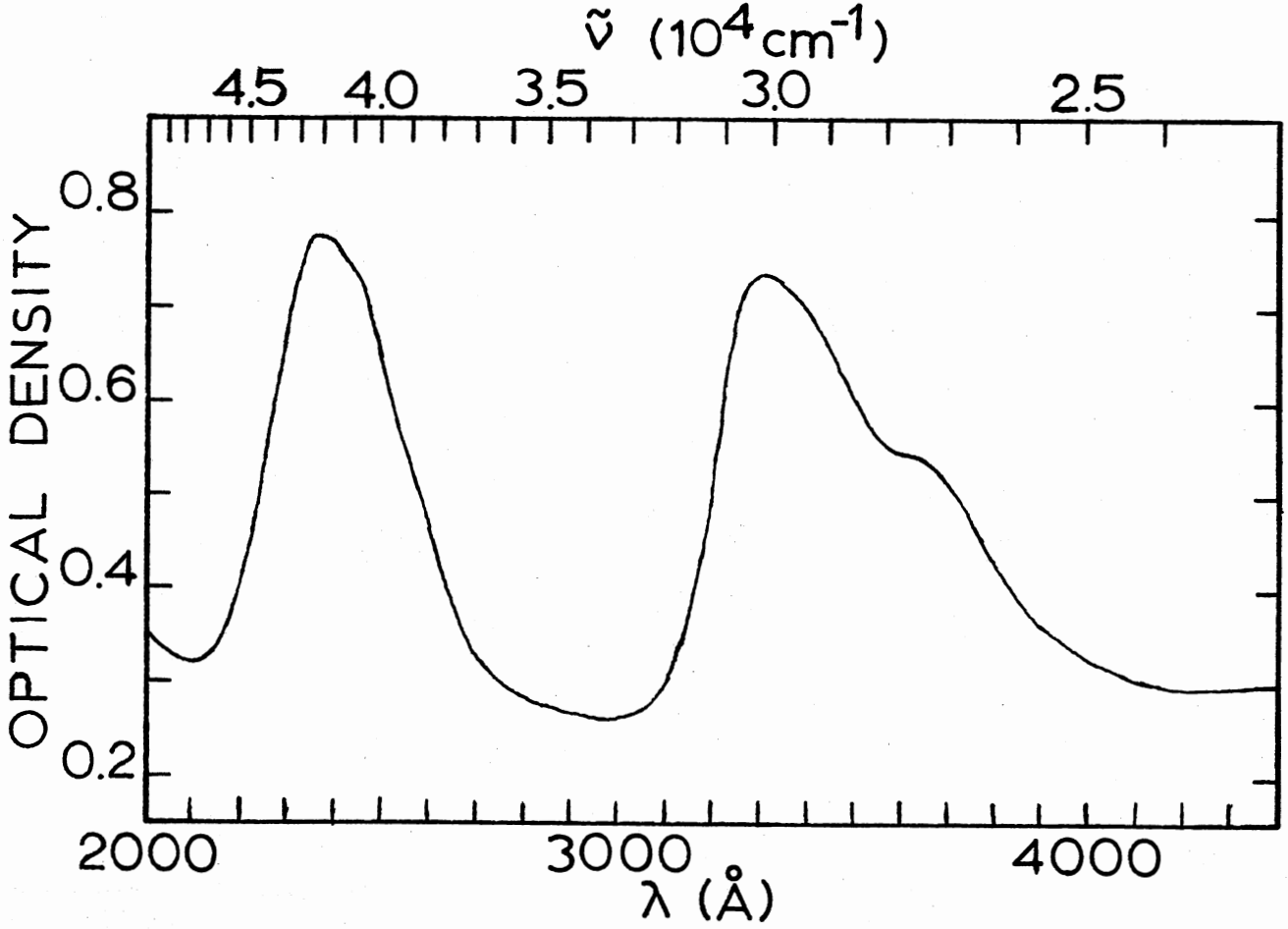

Figure 2. Room Temperature Absorption Spectrum

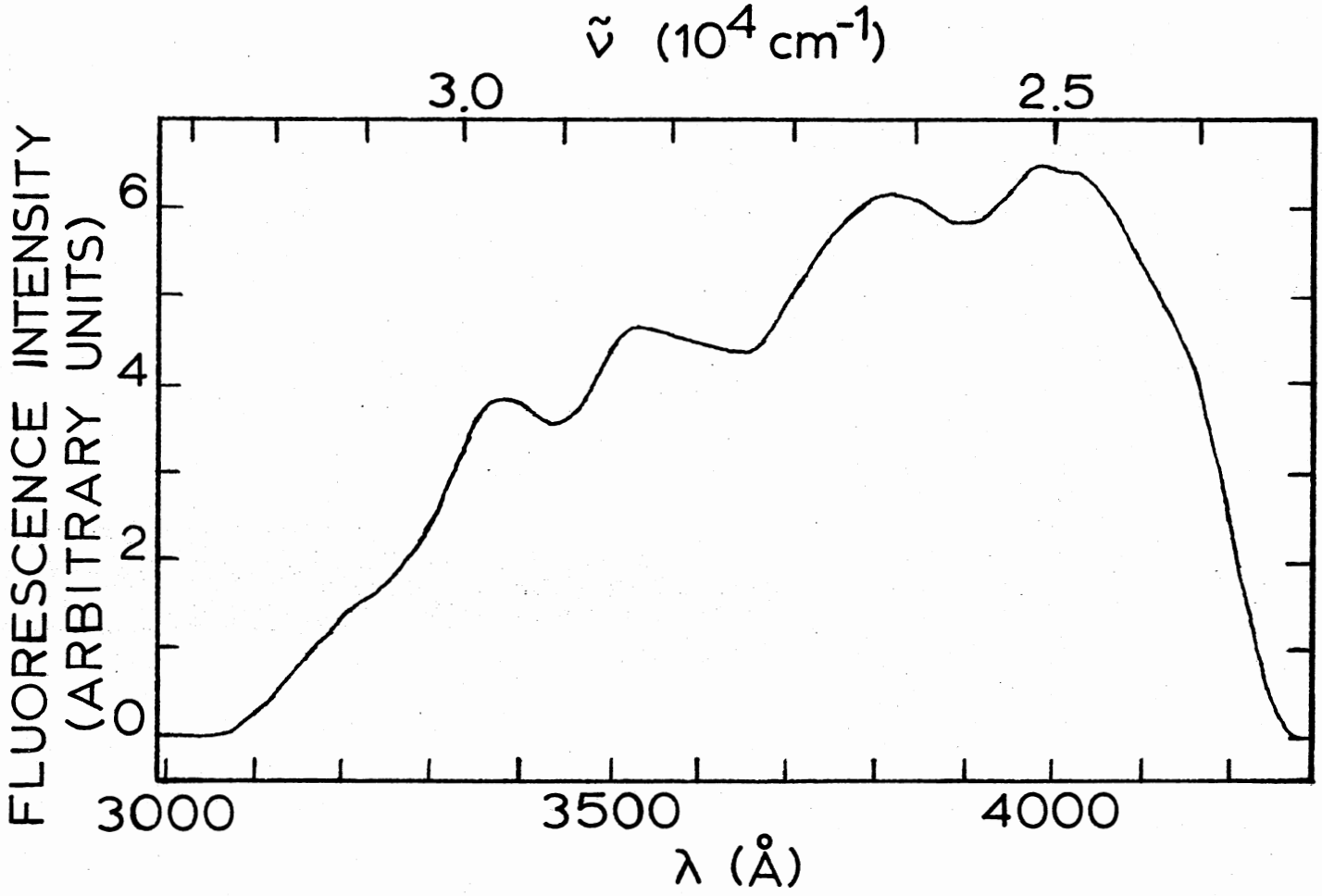

Figure 3. Excitation Spectrum for Observation at 4350Å at 13 K

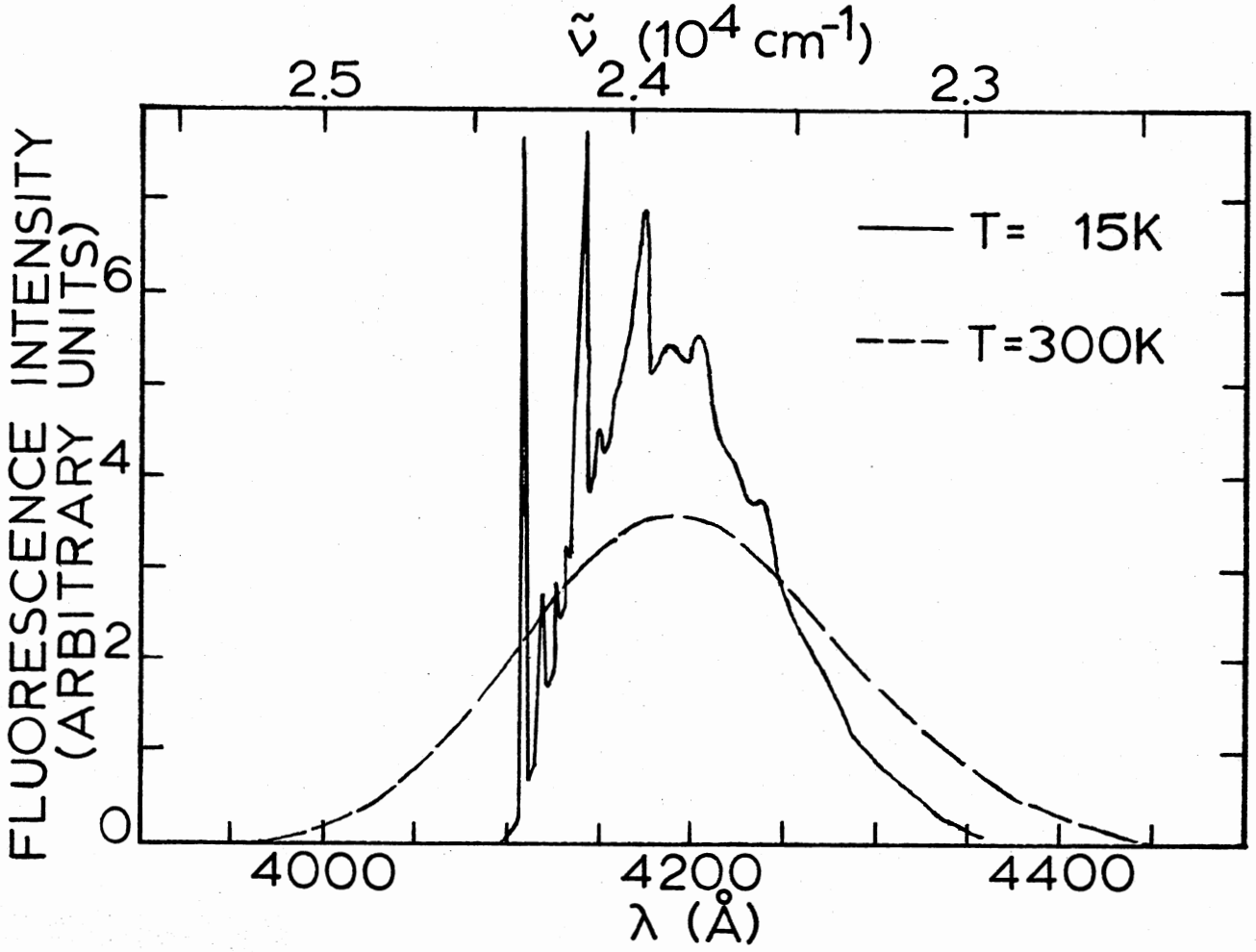

Figure 4. Fluorescence Spectra for 3371Å Excitation at 15 K and 300 K

a zero phonon line. This identification corresponds well with the interpretation of Tamura[8]. The fluorescence and excitation spectra were not corrected for equipment response, but correction is unnecessary due to the virtually flat response in the spectral region of interest.

The 13 K fluorescence spectra of the zero phonon line region are shown in Figure 5 for a sample stored at room temperature for several months and for a sample quenched from 600°C one day previous. Three sharp lines are observed. The quenched sample shows very little evidence of the line observed at 4103Å in the unquenched sample, and the 4095.5Å line is smaller relative to the 4107Å line by a factor of approximately three in the quenched sample. All fluorescence spectra in Figures 4 and 5 were monitored at a time after the laser pulse equal to or just later than the time of maximum intensity. All spectra of the zero phonon line region were taken using a Corning 7-51 color filter for the 4107Å line, which reduced its intensity by a factor of approximately seventeen.

Fluorescence lifetimes of the 4107Å and 4095.5Å lines of the quenched sample were measured at 13 K, 25 K, and 35 K. For the 4107Å line the lifetime decreases from 1.19 μs at 13 K to 1.04 μs at 25 K and 1.01 μs at 35 K, whereas the 4095.5Å lifetime is 0.88 μs at 13 K, 0.89 μs at 25 K, and 0.78 μs at 35 K. Although the precision of these measurements is limited, a slight decrease in lifetimes with increasing temperature is apparent. All decays appear purely exponential after approximately the first microsecond. Rise times were less than 0.1 μs.

Time Dependence of Spectra

Spectra of the zero phonon line region were taken at several times

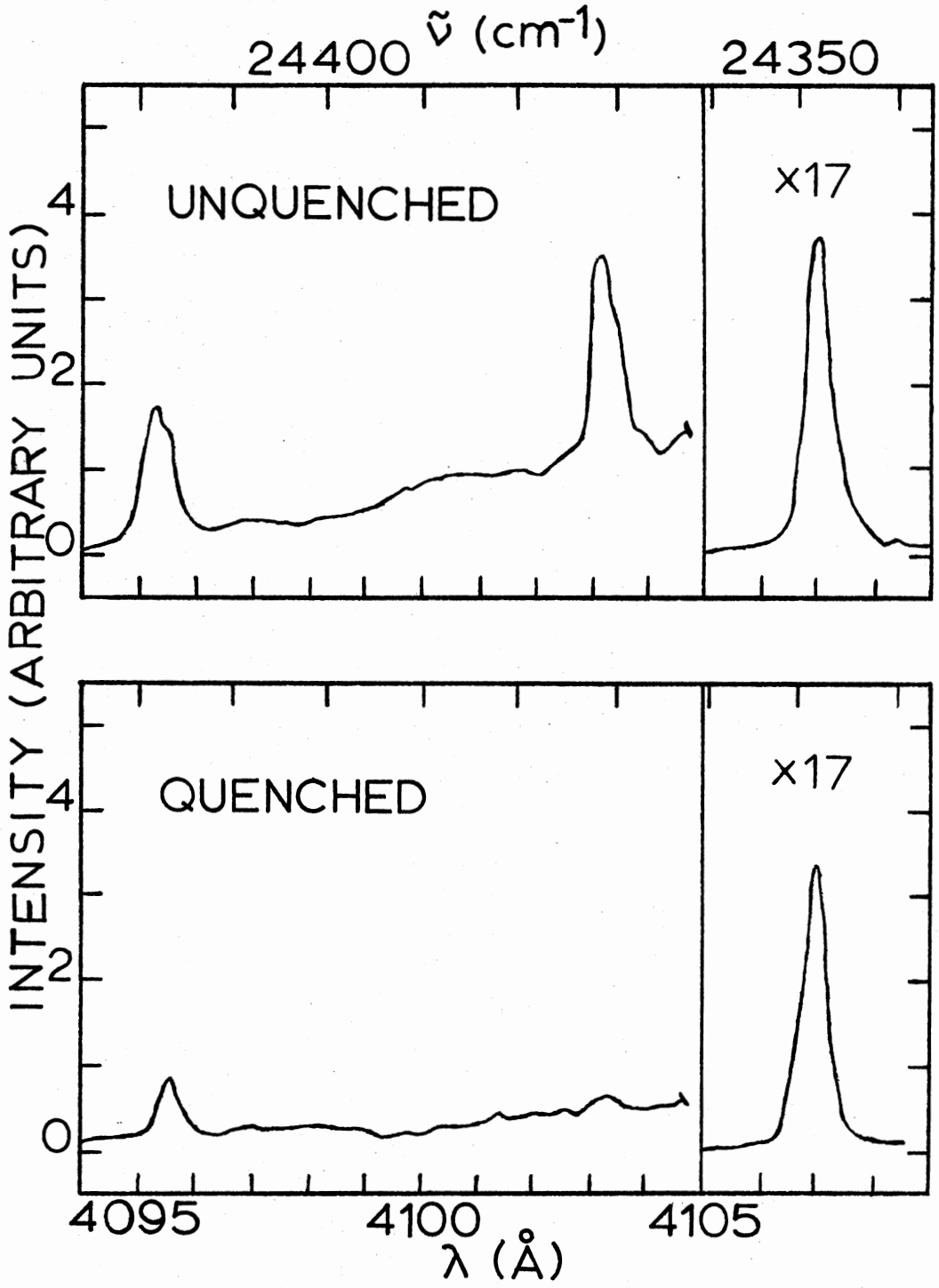

Figure 5. Zero Phonon Fluorescence Spectra at 13 K of Quenched and Unquenched Samples

after the laser pulse for temperatures of 13 K and 35 K. Broadening of the sideband with temperature, quite pronounced even at 35 K, obscured the 4095.5Å line for temperatures higher than that value. The lines are shifted to longer wavelength by about 0.3Å at 35 K as compared to 13 K, but little significance can be assigned to so small a shift. Spectra were also taken at two times after pulse at 25 K.

At 13 K spectra were taken at 0.01, 0.03, 0.1, 0.3, 1.0 and 2.0 μs after the laser pulse, whereas at 35 K the weaker signal allowed measurements only at 0.1 μs and later, that is only after the signal had reached maximum intensity. Further, there is a large uncertainty in the line intensities measured for the 2.0 μs point at 35 K, owing to the weakness of the signal at this long time after the pulse and the poorer signal to noise ratio encountered at the higher temperature. The shortest times must be taken as only approximate, as these very small delays after the laser pulse are comparable in size to the duration of the boxcar aperture, which was typically set at 50 ns but was shortened to about half that for the 0.01 and 0.03 μs runs. Two runs were made at each temperature and time after pulse except at 2.0 μs at 35 K, where only one usable run was obtained. Figure 6 shows the 13 K spectra of the quenched sample for times of 0.1 μs and 2.0 μs after excitation, from which a change in relative intensities of the 4095.5Å and 4107Å lines is observed.

Linewidths at half-height of the two measurable lines, those at 4095.5Å and 4107Å, were measured at each time after pulse at 13 K, showing no significant broadening with time, except at 2.0 μs, at which time linewidths are larger by about 50%. The average linewidths were 0.59Å for the 4095.5Å line and 0.58Å for the 4107Å line. Linewidth measure-

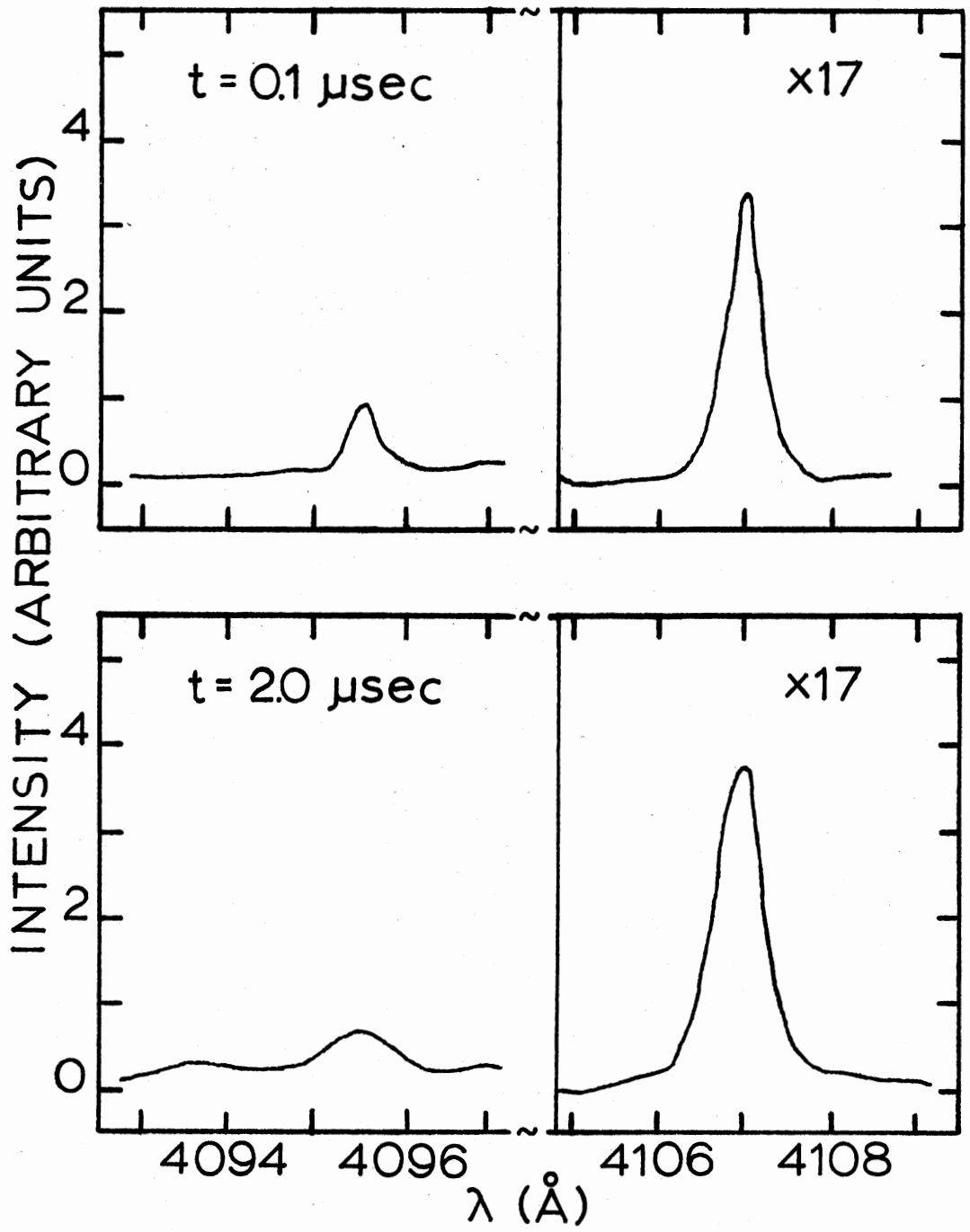

Figure 6. 4095.5Å and 4107Å Lines at 13 K at Two Times After Excitation

ments at 35 K, averaging 1.01Å at 4095.5Å and 1.17Å at 4107Å, were less accurate due to weakness of the 4095.5Å signal and use of wider, 35 μm, spectrometer slits to increase the signal. Linewidths were also measured at 25 K, where signal strength still allowed use of 10 μm slits, at 0.1 μs and 2.0 μs. No time dependence was seen, and the average linewidths were 0.72Å for the 4095.5Å line and 0.75Å for the 4107Å line. Linewidths are listed in Table I.

The integrated intensities of the 4105.5Å and 4107Å lines and the ratios of those intensities are also shown in Table I. Note that the two values in each column shown for 2.0 μs at 35 K do not represent two separate runs, but rather two extremal choices in integration of the spectral lines, given to indicate range of the uncertainty of this point as cited earlier. The intensity ratios are shown graphically in Figure 7. The low temperature ratios show an increase from 0.01 μs to 0.03 μs, then a small decrease to 0.3 μs followed by a strong increase. The increase in the ratio at long times reflects the difference in lifetimes between the two lines, that is, the ratio gets larger because the 4095.5Å intensity drops more quickly than the 4107Å intensity. The initial increase is probably due to a difference in rise times, indicating that the rise time of the 4095.5Å line, like its decay time, is shorter than that of the other line. The decrease of the intensity ratio at intermediate times thus cannot be due to a rise time or decay rate difference, and is attributed to energy transfer, as discussed in the next chapter.

The ratio of intensities at 35 K shows a stronger decrease with time after the laser pulse than does the lower temperature ratio. Due to the lack of short time data the initial rise is not seen, and the

TABLE I

INTEGRATED FLUORESCENCE INTENSITIES AND LINEWIDTHS

T (K)	t (μsec)	λ = 4095.5Å I	λ = 4095.5Å Δλ (Å)	λ = 4107Å I	λ = 4107Å Δλ (Å)	$\frac{I_{4107}}{I_{4095.5}}$
13	0.01	0.93	0.60	60.9	0.60	65.4
		0.85	0.64	63.8	0.60	75.1
	0.03	1.22	0.50	99.8	0.70	81.8
		1.08	0.50	96.6	0.58	89.4
	0.10	0.83	0.50	66.0	0.55	79.5
		0.72	0.60	62.7	0.54	87.2
	0.30	1.22	0.56	85.0	0.50	69.7
		1.33	0.50	81.6	0.50	61.4
	1.0	0.88	0.50	73.3	0.50	83.3
		0.82	0.59	73.6	0.50	89.8
	2.0	0.71	0.85	90.6	0.70	127.7
		0.76	0.77	91.1	0.65	119.8
25	0.10	1.02	0.75	90.6	0.75	87.9
	2.0	0.44	0.70	80.1	0.75	181.9
35	0.10	0.99	0.97	148.1	1.12	149.6
		0.86	-	134.5	1.00	156.4
	0.30	0.93	1.12	138.5	0.98	148.9
		0.96	-	136.2	0.96	141.8
	1.0	1.14	-	132.3	0.88	115.9
		1.21	0.94	146.5	1.03	121.0
	2.0	1.17	1.00	180.9	1.50	154.5
		1.32	-	167.4	-	126.8

($I_{4095.5}$ and I_{4107} in arbitrary units)

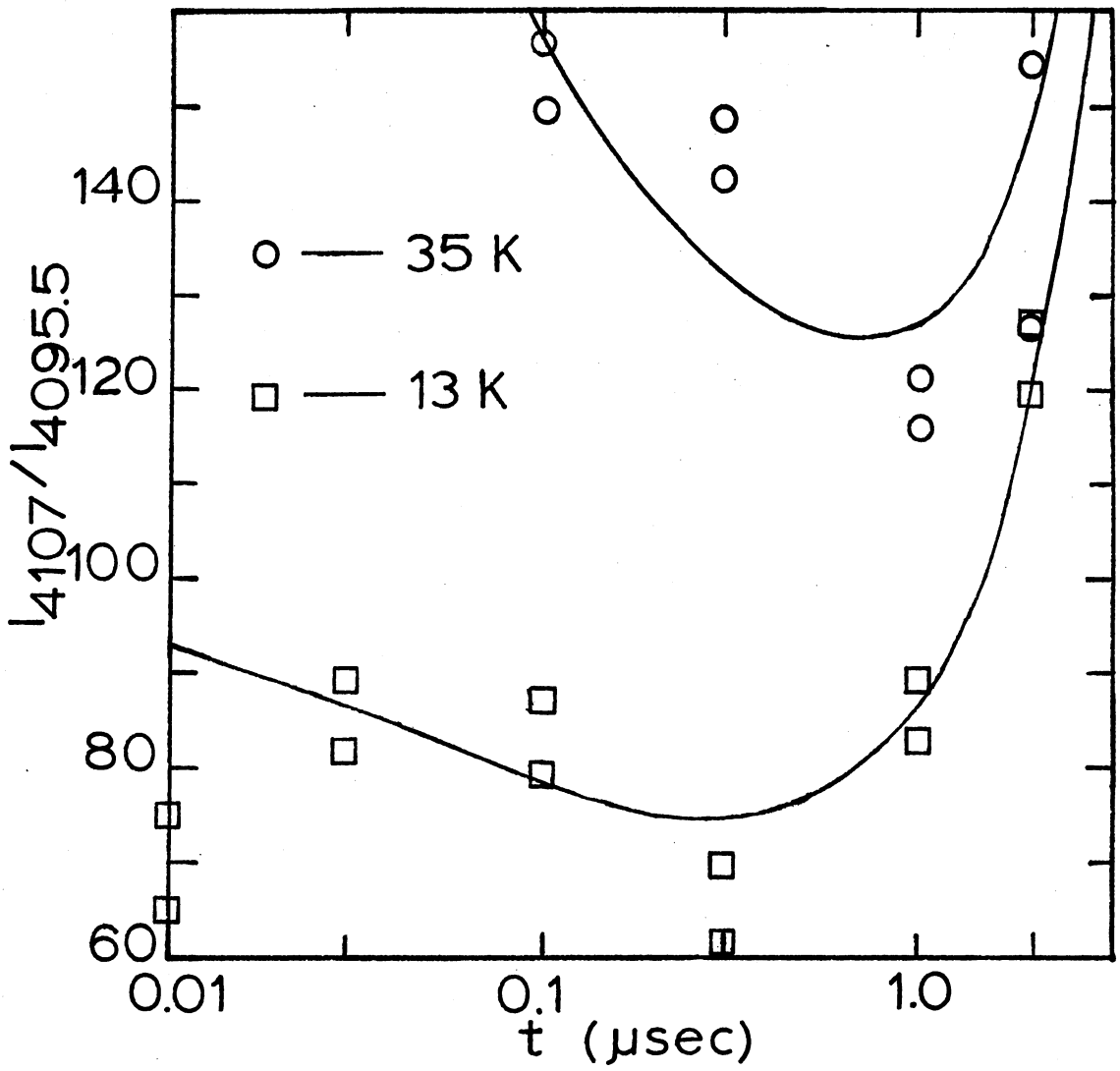

Figure 7. Time Dependence of the Integrated Fluorescence Intensity Ratio of the 4107Å to the 4095.5Å Line at 13 K and 35 K

decrease continues to 1.0 μs, rather than turning up after 0.3 μs as did the 13 K ratio. Although the 2.0 μs ratio has a large uncertainty, it clearly is larger than the 1.0 μs ratio, indicating that the lifetime difference between the two lines is beginning to dominate.

CHAPTER V

INTERPRETATION AND DISCUSSION

Introduction

Major features of the data which must be discussed include the difference in the sharp line spectrum between the quenched and unquenched samples, the lifetime difference between the two lines prominent in the quenched sample, and their different rise times. These may be explained in terms of the existence of different site symmetries for the Eu^{2+} ions in the crystal. In addition, the time dependence of the ratio of integrated intensities of the lines must be explained, and the interaction causing the time dependence must be characterized. These data may be understood if resonant energy transfer occurs between ions in the different crystal field sites.

Identification of Line Origins

It is assumed that the sharp lines at 4095.5Å, 4103Å, and 4107Å are all zero-phonon lines representing transitions from the lowest lying $4f^6 5d$ level to the ground state. The nitrogen laser used to excite the sample emits 3371Å light, which excites the europium ions into a higher level of the $4f^6 5d$ configuration. The ions then relax to the lowest level, from which fluorescence is observed. The rise times of the fluorescence signals, although short, are longer than the five ns duration of the laser pulse because some time is required for each ion to relax

from the higher level to the lower, metastable level. Since all fluorescence originates from the same ionic level, the existence of three zero phonon lines may be due to termination of the transitions on different levels of the split $4f^7$ ground state manifold, or to existence of different crystal field sites for each of which the energy levels are slightly different.

If different ground state levels are the source of the splitting the rise times and radiative lifetimes of the lines should not vary among the lines, since these characteristics depend on the excited state rather than the ground state. Neither the difference in rise times evidenced by the initial increase in the ratio of intensities at 13 K nor the measured difference in lifetimes supports this model.

The existence of different site symmetries for the europium ions may alter the strength of the electronic transition which gives rise to the fluorescence, resulting in a difference in lifetimes for the various sites. The energy level from which fluorescence occurs has been identified experimentally and by a simple coupling scheme as a Γ_8 level for Eu^{2+} in a fluorite lattice[2]. In that lattice the e_g crystal field orbital of the 5d electron is lower in energy, but in an alkali-halide lattice the t_{2g} orbital is expected to be below the e_g due to the six-fold coordination of the Eu^{2+} site. The same coupling scheme as that used by Chase[2], in which Coulomb interaction between the 5d and 4f electrons is regarded as small compared to the crystal field splitting of the 5d electron level and as compared to spin-orbit interaction and Hund's rules are used to order the spin-orbit multiplets, again predicts a lowest level of Γ_8 for the metastable state. Transitions from this state to the $^8S_{7/2}$ ground state are electric dipole allowed. The pres-

ence of charge compensating vacancies or clusters of europium ions would lower the symmetry of each site, but without specific knowledge of the type of sites existing in the sample, particular selection rules cannot be determined. However, it is reasonable to assume that the fluorescent transition from $4f^6 5d$ to the ground state is electric dipole allowed in each lower symmetry, as it is in the cubic, but that different possible environments of the Eu^{2+} ion can alter the strength of the transition. The observed lifetimes in $KCl:Eu^{2+}$, which are rather short and are not equal for the two lines, support these assumptions. Similarly, different environments may explain the observed difference in rise times. Thus, the time dependence of the data supports the identification of the different zero phonon lines as arising from sites of different symmetry.

Further support for this identification is found in the change of relative intensities of the zero phonon lines upon annealing and quenching of the sample. The decrease of intensity of the 4095.5Å line relative to the 4107Å line, and the large decrease of the 4103Å line relative to the others is not consistent with assignments of the lines to transitions terminating on different crystal field or spin-orbit split levels of the ground state, but may readily be explained as a change in relative populations of different site symmetries upon heat treatment. The annealing of the sample provides sufficient thermal energy to break up many aggregates of Eu^{2+}-cation vacancy pairs whereas the quenching of the sample to room temperature freezes the pairs for a time in their high temperature distribution, as discussed earlier. Thus, the 4103Å and 4095.5Å lines, which both decrease upon heat treatment, must be due to aggregates whose numbers are decreased by the thermal activation of annealing. The 4107Å line may be due to isolated europium-vacancy pairs,

whose number should increase as the clusters are broken up, or to a type of cluster less readily broken up by the high temperature. Positive identification of the site symmetries is not possible from these data, but the different behaviors of the three lines upon heat treatment strongly supports their association with three separate types of crystal field sites within the lattice.

The relative intensities of the lines also give some indication as to the relative number of ions in each type of site. Lifetime measurements indicate the decay probabilities per unit time of the 4095.5Å and 4107Å lines are comparable even though not equal, with the consequence that the ratio of intensities of these lines is comparable to the corresponding ratio of the numbers of excited ions in the two types of sites. Further, since the laser excitation wavelength is well into the broad observed excitation band, the small difference in the energy levels of the different sites indicated by the difference in wavelengths observed among the zero phonon lines probably has little effect on the strength of absorption of the exciting light by the different sites. Consequently, there is no reason to believe that one type of site was excited preferentially, and the intensity ratio should also be comparable to the ratio of the number of ions, excited and unexcited, in the corresponding crystal field sites.

Energy Transfer Model

The time dependence of the intensity ratios after 0.03 μs exhibits a decrease followed by a strong increase. The behavior may be fit by two simple models, one which attributes the decrease and subsequent increase to two different types of energy transfer and one which attributes

the decrease of the ratio to energy transfer but associates the increase with an intrinsic lifetime difference between the lines.

In the first model the decrease of the ratios is assumed to be due to resonant energy transfer, for which the probability is independent of the direction of transfer. Consequently, the net transfer proceeds from the ions in the more populous type of site to those in the less populous, thus accounting for the decrease of the intensity ratio toward unity. The second type of transfer in this model must not be due to a resonant interaction, for it drives the intensity ratio farther from unity. The rate of phonon assisted transfer is proportional to the probability of phonon emission for transfer from a high energy state to a low energy state, and thus is proportional to $n(w) + 1$, where $n(w)$ is the occupation number for phonons of frequency w[15]. For transfer from the lower to the higher energy state the rate is proportional to $n(w)$ since phonon absorption occurs. Since $n(w)$ is much smaller than one at low temperatures transfer by phonon emission must dominate, resulting in an increase in the number of excited ions in the lower energy site relative to the number in the higher energy site. This agrees with the time dependence of the data at long times.

The two types of energy transfer assumed in this model cannot occur between ions in the same two types of sites, for in such a case the stronger interaction would dominate at all times and the time dependence of the data would not be predicted. The two interactions must, therefore, be assumed to occur between different pairs of sites, one pair for which phonon assisted transfer dominates and another for which resonant transfer is stronger. However, this assumption supposes that one or both of the fluorescence lines is actually two lines, one from each of

two distinct site symmetries. Such accidental superpositon is unlikely, with the result that this model is also improbable.

The second model assumes only one type of energy transfer, a transfer which results in the observed decrease of the intensity ratio at intermediate times. This interaction is assumed to be resonant, as in the other model, to account for the apparent transfer from the lower energy, more populous type of site to the higher energy, less populous type. The increase in the intensity ratio at long times is attributed to a difference in the intrinsic lifetimes of the two lines which is assumed to dominate the time dependence of the energy transfer at sufficiently long times. The relative simplicity of this model and the greater plausibility of its assumptions make it preferable to the first.

The proposed energy transfer model is thus the second of the two discussed, and is depicted in Figure 8. W and W' are the rates of excitation of the higher energy site and the lower energy site respectively, and are taken as delta functions at time zero. Since finite rise times are observed, this simple form for excitation is not exact, but it is a good approximation since the rise times are rather short and must be used since quantitative information on the time dependence of the relaxation of the ions into the metastable state is lacking. B and B' are the fluorescence decay rates of the states with populations $n_a(t)$ and $n_s(t)$ respectively, and w is the rate of energy transfer, which is the same for transfer from activator, n_a, to sensitizer, n_s, or from n_s to n_a.

Rate Equations and Solutions

If the energy transfer occurs by diffusion or by a single step

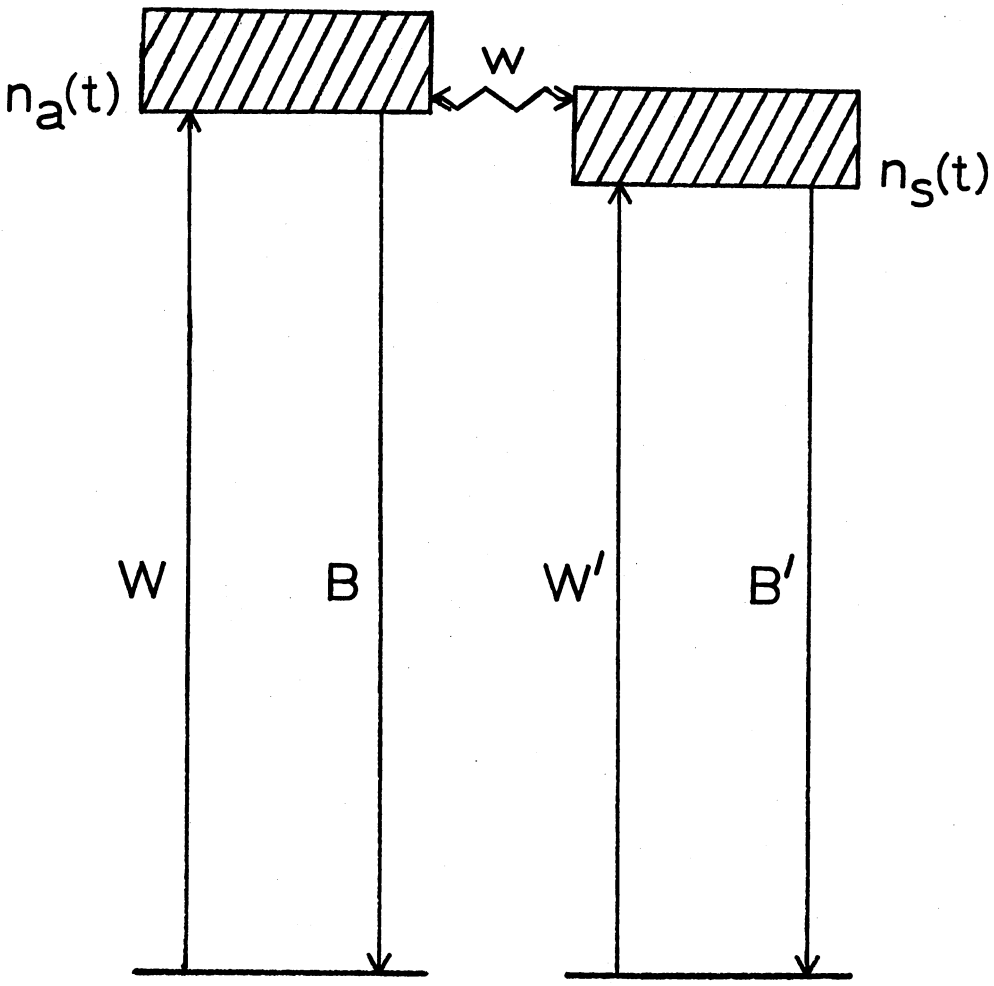

Figure 8. Proposed Energy Transfer Model

interaction between ions separated by a fixed distance, the transfer rate, w, is constant as seen in Equations (27) and (54). In this case the rate equations governing the populations $n_a(t)$ and $n_s(t)$ are

$$\dot{n}_a(t) = W - (B + w)n_a(t) + wn_s(t) \tag{55}$$

$$\dot{n}_s(t) = W' - (B' + w)n_s(t) + wn_a(t). \tag{56}$$

The solutions of this set of equations do not fit the data, however, as the difference in radiative decay rates simply acts to make the effective transfer probability in one direction larger than that in the reverse direction. Variation of the parameters changes the intensity ratio at which equilibrium is reached, but can never produce a minimum such as that observed experimentally.

If, however, the energy transfer occurs by a single step resonant process to sites distributed randomly in the sample, w is a function of time. For an interaction involving dipole allowed transitions such as encountered here it is reasonable to assume that the electric dipole-dipole interaction is the dominant transfer mechanism. Consequently, from Equation (44), $w_{random}(t) = w/t^{\frac{1}{2}}$ where the constant $w = 4\pi^{3/2}R_o C_a/3(\tau')^{\frac{1}{2}}$, and $\tau' = 1/B'$. In this case the rate equations become

$$\dot{n}_a(t) = W - Bn_a(t) - wn_a(t)/t^{\frac{1}{2}} + wn_s(t)/t^{\frac{1}{2}} \tag{57}$$

$$\dot{n}_s(t) = W' - B'n_s(t) - wn_s(t)/t^{\frac{1}{2}} + wn_a(t)/t^{\frac{1}{2}}. \tag{58}$$

This set of equations is very difficult to solve, but may be simplified if it is noted that $n_s(t)$ is always much larger than $n_a(t)$, as indicated by the consistently large intensity ratios observed. Consequently, little error is introduced by dropping the $wn_a(t)/t^{\frac{1}{2}}$ terms. The approximate rate equations are thus

$$\dot{n}_a(t) = W - Bn_a(t) + wn_s(t)/t^{\frac{1}{2}} \tag{59}$$

$$\dot{n}_s(t) = W' - B'n_s(t) - wn_s(t)/t^{\frac{1}{2}}, \tag{60}$$

which, with $W = n_{ao}\delta(t)$ and $W' = n_{so}\delta(t)$, give the ratio

$$\frac{n_s(t)}{n_a(t)} = \frac{e^{-(B-B')t_e - wt^{\frac{1}{2}}}}{n_{ao}/n_{so} + wA} \tag{61}$$

where

$$A = \int_o^{t^{\frac{1}{2}}} e^{(B-B')x^2} e^{-wx} dx. \tag{62}$$

The integral A was numerically computed for various times and parameter values using a simple trapezoid integration routine.

The intensity of fluorescence from each type of ion is proportional to the number of excited ions of that type and the radiative decay rate, B_r, so that

$$\frac{I_{4107}}{I_{4095.5}} = \frac{B'_r n_s}{B_r n_a} . \tag{63}$$

The radiative decay rate is not measured directly, but rather the total decay rate due to radiative and non-radiative mechanisms. However, at low temperatures for these ions the effects of non-radiative processes should be small and if the measured decay rates are used, B'_r/B_r is estimated to be about 0.75 at both 13 K and 35 K. Consequently, the ratio used to fit the data is

$$\frac{I_{4107}}{I_{4095.5}} = \frac{0.75\ e^{(B-B')t_e - wt^{\frac{1}{2}}}}{n_{ao}/n_{so} + wA} \tag{64}$$

From the measured lifetimes the difference in fluorescence decay rates is approximately 0.3 μs^{-1} at both temperatures, but since the ob-

served and the intrinsic decay rates need not be equal, B - B' must be taken as an adjustable parameter in fitting the data. The best fits at each temperature are plotted as solid lines in Figure 7, which also shows the measured intensity ratios. At 13 K the best fit is obtained with $B - B' = 0.9\ \mu s^{-1}$ and $w = 0.010\ \mu s^{-\frac{1}{2}}$, whereas the 35 K data are best fit by $B - B' = 0.7\ \mu s^{-1}$ and $w = 0.007\ \mu s^{-\frac{1}{2}}$. The best fit at 35 K is rather ill-defined, however, due to a lack of data points defining the long-time increase of the ratio.

Theoretical Transfer Rates

For a random distribution of activators the constant part of the transfer rate is, from Equation (44),

$$w = 4\pi^{3/2} R_o^3 C_a / 3\tau^{\frac{1}{2}}, \tag{65}$$

where for electric dipole-dipole resonant transfer

$$R_o^6 = \frac{3c^4 \hbar^4 Q_a}{4\pi\kappa^2 n^4} \left(\frac{\varepsilon}{\varepsilon_c}\right)^4 \int \frac{F_s(E) F_a(E)}{E^4}\, dE, \tag{66}$$

from Equations (26) and (27). The factor $\varepsilon^4/\varepsilon_c^4\kappa^2$ may be taken as one. Now $Q_a = \pi e^2 h f_a / mc$, where $f_a = mc/8\pi^2 e^2 \tilde{\nu}^2 \tau$ is the oscillator strength of the activator, and

$$\int F_s(E) F_a(E)\, dE = \frac{1}{hc} \int F_s(\tilde{\nu}) F_a(\tilde{\nu})\, d\tilde{\nu}. \tag{67}$$

Further,

$$\int \frac{F_s(E) F_a(E)}{E^4}\, dE \doteq \frac{1}{E_{ave}^4} \int F_s(E) F_a(E)\, dE. \tag{68}$$

Therefore R_o, the critical interaction distance, is given by

$$R_o^6 = \frac{3 f_a \phi_s}{4(2\pi n \tilde{\nu}_{ave})^4} \cdot \frac{e^2}{mc^2} \int F_s(\tilde{\nu}) F_a(\tilde{\nu})\, d\tilde{\nu} \tag{69}$$

in cgs units, where the quantum efficiency ϕ_s enters because the fluorescence lifetime, not the ionic radiative lifetime, is to be used. The oscillator strength may be estimated by comparison to the data and f value of Loh[16] for the 4f - 5d transition in Eu^{3+} to be about 5×10^{-2}. With this estimate, using n = 1.52, and assuming $\phi_s \doteq 1$, Equation (69) becomes

$$R_o^6 \doteq 3.578 \times 10^{-36} \times \int F_s(\tilde{\nu}) F_a(\tilde{\nu}) d\tilde{\nu} \tag{70}$$

with units of cm^6.

The integral of spectral overlap of the two fluorescence lines may be expressed as

$$\frac{1}{\pi} \cdot \frac{\Delta\tilde{\nu}_s + \Delta\tilde{\nu}_a}{(\Delta\tilde{\nu}_s + \Delta\tilde{\nu}_a)^2 + (\tilde{\nu}_s^o - \tilde{\nu}_a^o)^2} \tag{71}$$

For Lorentzian line shapes. Typically, observed lineshapes are neither Lorentzian nor Gaussian, but a convolution of the two. The Gaussian contribution is due to inhomogeneous broadening of the lines due to microscopic strains, and the Lorentzian contribution to homogeneous broadening such as by phonon interactions with the ions. Consequently the Lorentzian broadening occurs for each ion in the sample and may contribute to spectral overlap of the transitions of two ions. The observed lineshapes were analysed following the prescription of Posener[17], with the result that the Lorentzian linewidths are approximately 1.54 cm^{-1} for the 4107Å line and 1.48 cm^{-1} for the 4095.5Å line at 13 K, and 1.40 cm^{-1} for both lines at 25 K. As seen in Figure 9, the baseline of the fluorescence spectrum in the zero phonon region slopes much more at 35 K than at 25 K, indicating that the vibronic sideband broadens significantly in that temperature interval. Thus, phonon interaction with the electronic transitions of the ions appears to be more important at 35 K

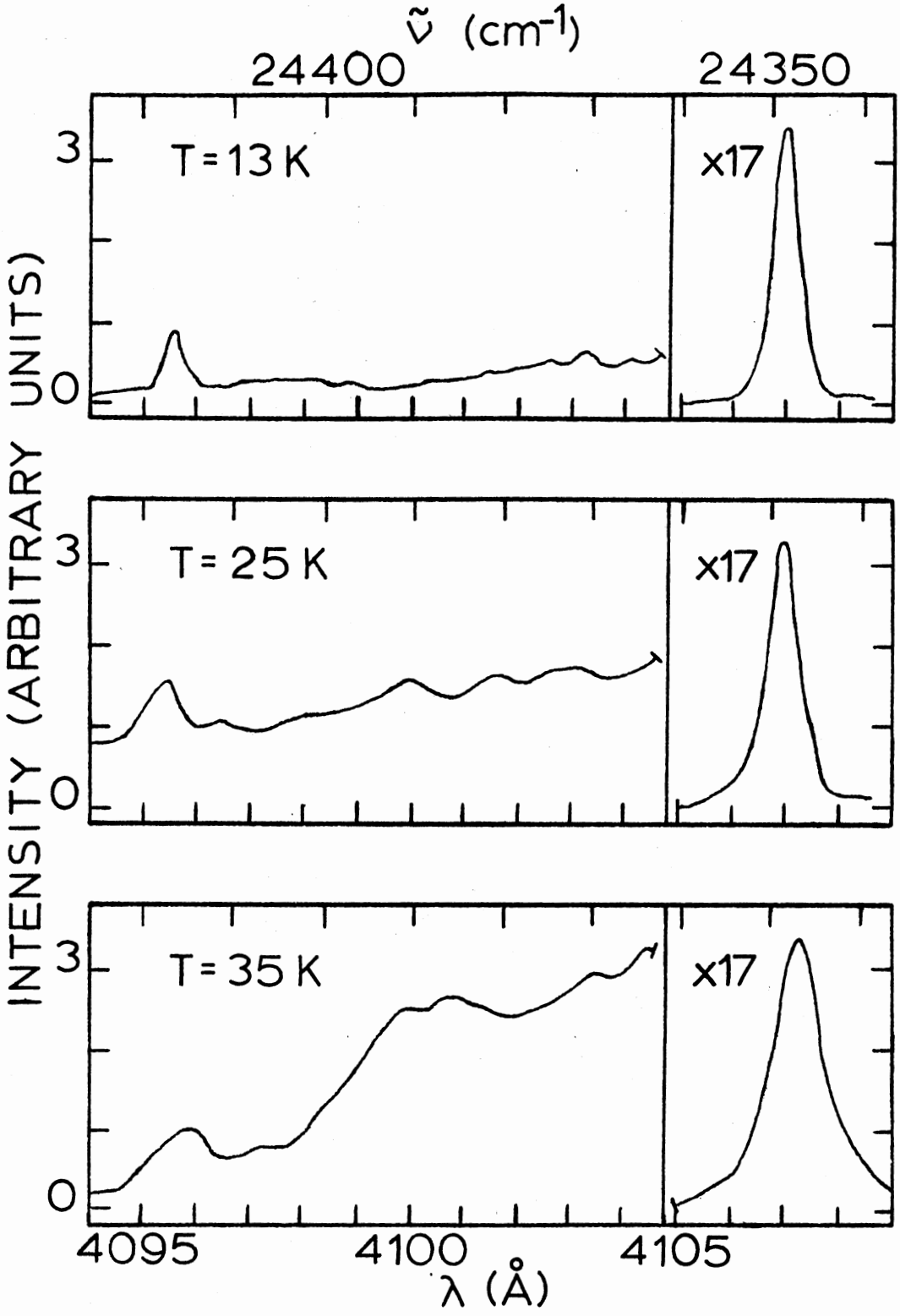

Figure 9. Zero Phonon Spectra at 0.1 μs After Excitation at Three Temperatures

than at 25 K so that it cannot be assured that the Lorentzian linewidths change as little in this temperature interval as in the 13 K to 25 K interval. The observed linewidths at 35 K may be broadened by the use of wider spectrometer slits, but this broadening contributes to the Gaussian component of linewidth rather than the Lorentzian, with the consequence that analysis of the 35 K line shapes still gives a reasonable estimate of the Lorentzian linewidths. This analysis was performed for the 4107Å line, yielding a linewidth of about 3.2 cm^{-1}. Because the 4095.5Å line at 35 K is not sufficiently larger than background noise to allow accurate measurement of linewidths, this value is assumed for the 4095.5Å line as well.

Calculations of the transfer rate constants at 13 K and 35 K from these values may be made if the measured 4107Å lifetimes are used for τ and if a suitable estimate of C_a is made. The best fit to the 13 K data was attained with $n_{so}/n_{ao} = 140$. At 35 K this ratio is much larger, but the growth of the sideband with temperature indicates that vibronic interactions may be important in altering the relative intensities of the zero phonon lines at this temperature. Consequently, the ratio of n_{so} to n_{ao} at the lowest possible temperature must be used to estimate the ratio of initially excited populations of the two sites, to minimize such thermal effects. If it is assumed that the laser does not pump either site preferentially, an assumption made plausible by the broad nature of the observed excitation and absorption spectra, C_a may be estimated to be $C_{Eu}/140$. Values of w thus calculated are shown in Table II, together with the theoretically estimated R_o's, Lorentzian linewidths, values of the fitting parameters, and R_o's calculated from the fittings by Equation (65), for temperatures of 13 K and 35 K.

TABLE II

ENERGY TRANSFER PARAMETERS FROM FITTINGS
AND THEORETICAL ESTIMATES

Parameter	T = 13 K	T = 35 K
n_{so}/n_{ao}	140	350
$B - B'$ (μs^{-1})	0.9	0.7
$\Delta\tilde{\nu}_{L4095.5}$ (cm^{-1})	1.48	3.2
$\Delta\tilde{\nu}_{L4107}$ (cm^{-1})	1.54	3.2
w_{fit} ($\mu s^{-\frac{1}{2}}$)	0.010	0.007
w_{theory} ($\mu s^{-\frac{1}{2}}$)	0.0058	0.0092
R_{ofit} (Å)	36.0	31.1
$R_{otheory}$ (Å)	30.0	34.0

Discussion

The curves obtained from the rate equation solution, Equation (64), provide a reasonable qualitative fit to the data if the rise time is ignored, as assumed in this model. A large difference between the B - B' values obtained from the fittings and the measured total decay rate dif-

ference is apparent. However, if energy transfer is neglected so that the intensity ratio is proportional to $\exp(B - B')t$, the change of the ratio of intensities from 1.0 μs to 2.0 μs is fit rather well with $B - B' = 0.3\ \mu s^{-1}$. Thus, the larger B - B' needed to fit the model is not due to a discrepancy between the lifetime measurements and the time resolved spectra, but rather it is due to the energy transfer which alters the observed decay rates. The magnitude of the difference between B - B' and the observed decay rate difference may also be due in part to the neglect of energy transfer from activator to sensitizer and to the inaccuracy of the numerical integration of A in Equation (64).

The agreement between the theoretically calculated value of w and that obtained from fitting of the data is reasonable, but whereas the theoretical w increases with temperature the w from fitting is smaller at 35 K than at 13 K. The smaller value at 35 K is found, despite the fact that energy transfer continues to dominate the intensity ratio for a longer time than at 13 K, due to the largeness of the initial ratio. If there are many more excited sensitizers than activators the difference in populations gives a large total transfer of energy even if the interaction strength is rather small.

However, there is no reason to expect the relative number of initially excited ions at the two crystal field sites to be significantly different at the two temperatures. The ratio of intensities at 0.1 μs changes very little from 13 K to 25 K, at which temperatures the slope of the baseline of the spectrum is also very similar, whereas a large difference is evident at 0.1 μs between the 25 K and 35 K data. At 35 K the slope and structure of the baseline also indicate a significant growth of the vibronic sideband into the zero phonon region of the spec-

trum, so that coupling of the ionic transitions to phonons must be significantly stronger than at the lower temperatures. Since ions at different crystal field sites may well couple differently to lattice vibrations, the change in intensity ratio of the zero phonon lines with temperature may be due to a different change in the zero phonon line intensity relative to its sideband intensity for each of the types of sites. If the 13 K ratio of n_{so} to n_{ao} is assumed to be more closely indicative of the true ratio of ion populations at both temperatures, the minimum of the intensity ratio occurs at 1.0 μs for an w of roughly 0.016 $\mu s^{-\frac{1}{2}}$ for B - B' = 0.7 μs^{-1}. The value of w required to fit the data varies significantly as B - B' is changed, 0.7 μs^{-1} being chosen because that value had given the most reasonable fit in the previous 35 K fitting. For this value of w R_o is 40.9Å, and for any choice of B - B' the value of w must be larger to produce a minimum of the ratio at 1.0 μs than at 0.3 μs, in agreement with the increase of the theoretical w from 13 K to 35 K. That the measured value of w is larger than the theoretical estimate tends to rule out interaction mechanisms of higher order than electric dipole-dipole, as such mechanisms would tend to predict an even smaller transfer rate. The interaction must, therefore, be electric dipole-dipole, with the discrepancy probably due to the approximate values used for f_a and other parameters.

It may be noted that the increase of linewidths of the two zero phonon lines at 2.0 μs at 13 K gives possible evidence of the occurrence of energy transfer among ions of the same site symmetry. As energy is passed among ions in the crystal, regions of microscopic strain not originally excited may be encountered, thus increasing the inhomogenous broadening of the lines as a function of time. However, similar time-

dependent broadening is not observed at 25 K and only the 4107Å line exhibits such a broadening at 35 K, so that such an interpretation is not certain.

CHAPTER VI

SUMMARY AND CONCLUSIONS

Time resolved spectroscopy has been used to study the time dependence of the zero phonon fluorescence spectrum of divalent europium in a potassium chloride host. Spectra of an annealed and quenched sample were compared to those of a sample kept at room temperature for several months, and time dependent data were taken on the quenched sample at three temperatures. From lifetime measurements and comparison of the quenched and unquenched samples the three observed zero phonon lines were attributed to the same ionic transition in Eu^{2+} ions of different site symmetry. The relative intensities of the 4095.5Å and 4107Å lines, the two lines measurable in the quenched sample, were observed to vary with time after laser excitation in a manner which may be explained in terms of a difference of radiative decay rates for ions at the different crystal field sites and the transfer of energy between ions of the two site symmetries. The data were found to be consistent with single step resonant transfer of energy by electric dipole-dipole interaction between randomly distributed sensitizers and activators. At a temperature of 13 K fitting of the integrated intensities data gave a critical interaction distance of R_o = 36.0Å, in reasonable agreement with the theoretical estimate of 30.0Å. At 35 K a direct fit to the data yielded R_o = 31.1Å, but with a more reasonable estimate of the ratio of initially excited ions in the two site symmetries an approximate R_o of 40.9Å was

obtained, compared to a theoretical estimate of 34.0Å. The increase of the theoretical R_o with temperature is thus paralleled by that obtained from the fittings, with agreement at both temperatures sufficient to support the proposed energy transfer model.

Additional study of this material should include a careful analysis of the site symmetries present, in view of the tendency of the Eu^{2+} ions to aggregation. Mechanical strengths data indicate that many hours of anneal time are required to attain a state of little or no aggregation, with the result that the strong zero phonon fluorescence line observed after a much shorter anneal time may not be due to an isolated Eu^{2+}-cation vacancy pair[11]. If the type of configuration giving rise to this line can be determined not to be the simple Eu^{2+}-vacancy pair the vibronic sideband of the line may be analysed with coupling of phonons to the appropriate Eu^{2+} site symmetry taken into account, as previous work has assumed the isolated ion and nearest-neighbor vacancy configuration in analysis of the sideband[8].

REFERENCES CITED

1. Reisfeld, R. and A. Glasner, J. Opt. Soc. Am. 54, 331 (1964).

2. Chase, L. L., Phys. Rev. B2, 2308 (1970).

3. Loh, E., Phys. Rev. 175, 533 (1968).

4. Kisliuk, P., H. H. Tippins, C. A. Moore, and S. A. Pollack, Phys. Rev. 171, 336 (1968).

5. Weakliem, H. A., Phys. Rev. B6, 2744 (1972).

6. Fong, F. K., Phys. Rev. 187, 1099 (1969).

7. Fong, F. K., R. L. Ford, and R. H. Heist, Phys Rev. B2, 4202 (1970).

8. Nasu, K., A. Tamura, K. Kojima, and T. Kojima, J. Phys. Soc. Japan 36, 55 (1974).

9. Dexter, D. L., J. Chem. Phys. 21, 836 (1953).

10. Powell, R. C., Phys. Rev. B2, 1207 (1970).

11. Martin, J. and E. Sill, Private Communication.

12. Young, M. and L. Halliburton, Private Communication.

13. Naberhuis, L. and F. K. Fong, J. Chem. Phys. 56, 1174 (1972).

14. Sundberg, M. N., H. V. Lauer, and F. K. Fong, J. Chem. Phys. 62, 1853 (1975).

15. Orbach, R., in Optical Properties of Ions in Crystals, edited by H. M. Crosswhite and H. W. Moos (Wiley-Interscience, N. Y., 1967), p. 445.

16. Loh, E., Phys. Rev. 147, 332 (1966).

17. Posener, D. W., Australian J. Phys. 12, 184 (1959).

VITA

Larry Dean Merkle

Candidate for the Degree of

Master of Science

Thesis: ENERGY TRANSFER IN EUROPIUM DOPED POTASSIUM CHLORIDE

Major Field: Physics

Biographical:

Personal Data: Born in Tulsa, Oklahoma, July 14, 1952, the son of Mr. and Mrs. H. E. Merkle.

Education: Graduated from Nathan Hale High School, Tulsa, Oklahoma, in May, 1970; enrolled at North Texas State University, 1972; received Bachelor of Science degree from Oklahoma State University in 1974; enrolled in graduate program at the University of Illinois, 1974; completed requirements for the Master of Science degree at Oklahoma State University in May, 1976.

Professional Experience: Undergraduate research assistant, North Texas State University, 1972; undergraduate research assistant, Ames Laboratory, 1973; undergraduate teaching assistant, Oklahoma State University, 1973-74; graduate teaching assistant, University of Illinois, 1974; graduate research assistant, Oklahoma State University, 1974-75; graduate teaching assistant, Oklahoma State University, 1975-76.